Solid-State NMR of Nanomachines Involved in Photosynthetic Energy Conversion

A. Alia, Francesco Buda, Huub J.M. de Groot, and Jörg Matysik

Solid State NMR, Leiden Institute of Chemistry, Leiden University, Leiden 2300 RB, The Netherlands; email: a.alia@chem.leidenuniv.nl, f.buda@chem.leidenuniv.nl, groot_h@chem.leidenuniv.nl, j.matysik@chem.leidenuniv.nl

Keywords

Abstract

Magic-angle spinning NMR, often in combination with photo-CIDNP, is applied to determine how photosynthetic antennae and reaction centers are activated in the ground state to perform their biological function upon excitation by light. Molecular modeling resolves molecular mechanisms by way of computational integration of NMR data with other structure-function analyses. By taking evolutionary historical contingency into account, a better biophysical understanding is achieved. Chlorophyll cofactors and proteins go through self-assembly trajectories that are engineered during evolution and lead to highly homogeneous protein complexes optimized for exciton or charge transfer. Histidine-cofactor interactions allow biological nanomachines to lower energy barriers for light harvesting and charge separation in photosynthetic energy conversion. In contrast, in primordial chlorophyll antenna aggregates, excessive heterogeneity is paired with much less specific characteristics, and both exciton and charge-transfer character are encoded in the ground state.

Contents

Chlorophyll (Chl): the most abundant and significant dye molecule for harvesting light; involved in charge separation

Reaction center (RC): complex of proteins that performs light-induced charge separation for driving the chemical reactions needed to store energy

PSI, PSII: photosystem I, photosystem II

Photosynthesis: the process that converts light to store energy by chemical synthesis in plants, algae, and some bacteria

INTRODUCTION

Photosynthetic energy conversion processes evolved three billion years ago in plants, algae, and microorganisms. They are the principal source of free energy needed to sustain the biosphere with green plants and algae, which split water and concentrate CO_2 from the air. Photosynthetic energy conversion operates with a limited number of molecular components, and the diversification is in the details of the physics and physical chemistry of the molecular building blocks; of the spatial, electronic, and vibrational structure of the chlorophyll dyes; and of how they are assembled with the polypeptide chains to form responsive matrices. The matrices are capable of classically coherent evolution for the kinetic stabilization and accumulation of exciton and charge transfer intermediates for efficient light harvesting, charge separation, and catalysis in spatially well-organized photosynthetic membranes (7, 23) (**Figure 1**). The protein scaffoldings and pigment arrangements of reaction centers (RCs) are similar for the two classes of photosystems, including photosystems I and II (PSI, PSII), which have evolved to drive oxygenic photosynthesis by working in tandem at different redox potentials to bridge the free energy gap between H_2O and H_2 or carbohydrate fuel from CO_2 in the air.

Although photosynthetic proteins and pathways are conserved in evolution and across taxonomic boundaries, the steady state of photosynthetic conversion varies considerably across species, genotypes, and phenotypes and adapts to light intensity, CO_2 concentration, nutrient supply, heat, or drought, among others. For instance, the thylakoid membrane shown in **Figure 1** can protect itself against high light intensity by transitioning between photochemically active and nonphotochemical quenching states, triggered by a proton gradient (32). Without protective losses,
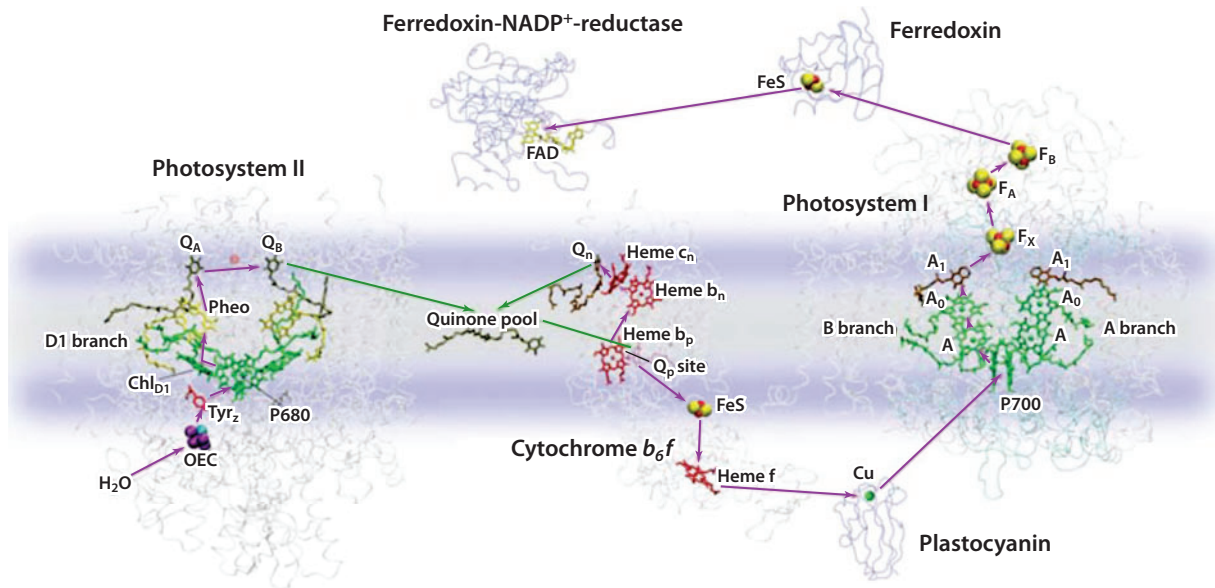
Figure 1

Energy is central to photosynthesis, and photosynthetic membranes contain electron and proton pumps driven by the energy of light. The figure provides a schematic view of a photosynthetic membrane, the thylakoid membrane, for oxygenic photosynthesis. Here photosystem I and photosystem II operate in tandem to extract electrons from water and produce energy carriers from dilute atmospheric CO_2 via the carbon-fixing reactions of the Calvin-Benson cycle. According to recent insights from structural biology, photosystem I and photosystem II have a similar architecture and may share a common biological origin. Embedded in the photosystem are the cofactors, and most prominent are the chlorophylls, which occur in different varieties across taxonomic boundaries. Abbreviation: Pheo, pheophytin.

photosynthetic conversion operates close to the efficiency maximum that is thermodynamically feasible, according to the detailed balance limit of linear nonequilibrium photochemical conversion (15, 71).

The chemical kinetics of photosynthesis allows for transient accumulation of intermediates at increasing timescales and decreasing free energy, in conjunction with the production of mixing entropy in the chemical storage network (15). In oxygenic photosynthesis, four positive electronic charges are accumulated on the timescale of water oxidation catalysis, $\sim 10^{-3}$ s, which is six orders of magnitude longer than the $\sim 10^{-9}$ s fluorescence lifetime of the chlorophyll cofactors. In parallel, delocalization is strongly reduced, as many antenna chlorophylls feed into an RC, and the effect of four photons is concentrated to extract four electrons from two small water molecules. A matching of timescales, length scales, and energy scales in the photosynthetic membrane architecture to its protein complex constituents leads to a smoothly functioning nanomachine comprising photosynthetic antennae for rapid long-range exciton transfer on the nanosecond timescale, RCs for electron hole separation on the microsecond timescale, and stabilization of positive-charge accumulation by proton release on the millisecond timescale in a $MnCaO_4$ catalytic site (51).

The protein complexes lower the transition states and energy barriers for optimal chemical energy conversion (15). In recent years we have developed and applied magic-angle spinning nuclear magnetic resonance (MAS NMR) methods for resolving chemical preprogramming by protein-induced misfits and associated activation dynamics for barrier-less light harvesting and charge separation (13, 52). This line of research addresses the design that is intrinsic to biology

Antennae: harvest light by transfer of excitations to reaction centers

Magic-angle spinning (MAS): a method to obtain NMR spectra from solid samples at high resolution

Nuclear magnetic resonance (NMR) spectroscopy: a common research tool used to determine the structure of molecules and their physicochemical characteristics by irradiating them with radiowaves and detecting the nuclear responses

and is established by evolution in a historically contingent manner, where apparent paradoxes are exploited by biology for engineering and optimizing processes. Although chlorophyll cofactors can both support transfer of long-living excitons in antennae and perform rapid charge separation in RCs, the physical requirements for both processes are conflicting. On the one hand, long-living excitons require bound electrons and holes with little charge-transfer character because this shortens the exciton lifetime. On the other hand, rapid charge separation requires unbound electrons and holes. When light is abundant and photosynthesis works against environmental constraints such as low CO_2 concentration in the atmosphere, e.g., in the case of oxygenic photosynthesis, which developed later in evolution, throttling of the conversion chain is necessary, introducing an evolutionary selection pressure to keep excitons alive and to stabilize separated charges. Early in the evolution of photosynthesis, light was scarce and individual chlorophylls might receive less than one photon per day. Nature has developed special chlorosome antennae for low light that contain heterogeneous protein-free chlorophyll aggregates. These aggregates are thought to exploit charge-transfer character in the antenna function to produce a very large dipole moment for fast long-range Förster transfer into a membrane-bound, antenna-RC complex on a timescale shorter than the exciton lifetime (22, 52). At later stages, evolutionary selection pressure led to optimization of exciton transfer properties in antenna systems, and to optimization of charge transfer properties in RCs, by shaping of cofactors and by their embedding in highly ordered responsive protein matrices (15). Interaction between bottom-up and top-down causality, which is characteristic of biology, leads to biological engineering and adaptation by diversification as the basis to serve selection from the higher levels of the biological hierarchy.

The classification of mechanisms of function, with the idea of a contingent evolutionary timeline in the background to complement physical and chemical principles, goes beyond the common practice of the physical sciences in general and structure determination by solid-state NMR in particular. It is, however, well in line with the unbiased approach of biophysics for investigating genuine biology by physical and physicochemical intuition, supported by observations rather than hypotheses, to allow for the unexpected that is characteristic of biological diversity (30). We consistently build on evidence collected with solid-state NMR spectroscopy and use first-principles-constrained molecular modeling as a tool to bridge diffraction data for the structure to the physical and physicochemical data available for the characterization of reaction coordinates. This approach allows us to recognize physical relations and common denominators in mechanisms of function (30).

One important common denominator in photosynthesis is the similar architecture of RCs (27). Because antenna systems are diverse, they provide invaluable information about chemically preprogramming chlorophyll cofactors, which contributes to the foundation of RC studies as well (15, 52). For RC studies we have developed and extensively used photo-CIDNP (chemically induced nuclear polarization) solid-state NMR. This powerful tool provides selective excitation of cofactors, yields electron density profiles in the ground state from the chemical shifts, yields excited state profiles from the signal intensities, gives insight into the kinetic stabilization of intermediates when used in a time-resolved manner, and, as of very recently, provides access to molecular dynamics from correlation signals in two-dimensional dipolar spectroscopy (14).

PROTEIN-FREE LIGHT HARVESTING IN CHLOROSOME ANTENNAE

The largest, fastest, and most efficient antennae in nature are chlorosomes (22). Chlorosomes contain hundreds of thousands of bacteriochlorophyll (BChl) *c*, *d*, or *e* pigments that are self-assembled to form oblong light-harvesting bodies. Solid-state NMR analyses have confirmed that chlorosome antennae are built from protein-free BChls in well-ordered microdomains (6, 25).

The domains form very large and compositionally heterogeneous organelles. Although solid-state NMR is rapidly developing as a method to determine molecular structure bottom-up, working from abundant distance constraints at the molecular level, resolving the structure of chlorosomes required a novel approach to bypass the heterogeneity and to establish a connection between the well-ordered microdomains and the supramolecular scaffolding that is the basis of the elongated antenna organelles (25).

Chlorosomes Are Built from Coaxial Cylinders of BChl with Functional Heterogeneity from Dislocations

In recent years, many photosynthetic species have been sequenced, including the green sulfur bacterium *Chlorobaculum tepidum*, which has chlorosomes that contain BChl *c* (8). The biosynthesis pathways of the BChls are known, and in the last stages of biosynthesis, steric crowding is enhanced (28). In particular, the BChl *c* that is formed by complete methylation of the C-20 is sterically more crowded than BChl *d* without the C-20 methyl, while partial methylation of the C-8 ($\sim$30%) and the C-12 ($\sim$90%) leads to increased heterogeneity and bulkiness in these side chains, which helps broaden the optical absorption profile for light harvesting (42). Recent advances in understanding the biosynthesis of BChl *c* have allowed researchers to construct a well-characterized *bchQ bchR bchU* (*bchQRU*) *C. tepidum* triple mutant that synthesizes well-defined, extended chlorosomes with more than 95% 17^2-farnesyl-*R*-[8-ethyl, 12-methyl] BChl *d* (28). Hence, when the final methylation steps are eliminated and the biological evolution is partially reversed, the highly heterogeneous BChl *c* pigment chlorosomes of *C. tepidum* are converted to homogeneous unmethylated BChl *d* chlorosomes with neat NMR spectra, showing essentially only one spectral component with narrow, well-resolved resonances in ultra-high magnetic fields (25). By collecting sparse distance constraints, Ganapathy et al. (25) identified a pseudosymmetric *syn-anti* parallel stacking mode of the BChl by using solid-state NMR (**Figure 2g,h**). The macrocycles alternate their orientation while the OH functionality that coordinates to the central Mg^{2+} ion of the next chlorophyll always points in the same direction along the stack (25). This dichotomy indicates that the chlorophylls are in a quasi- or pseudosymmetric stacking arrangement (25). By computational integration of NMR data with imaging results obtained by electron microscopy, researchers determined a set of templates for chlorosome scaffolding and structural variability that provide a detailed view of the structural basis of the biological light-harvesting function for the chlorosome antenna class (24, 25) (**Figure 2a–b**). In the Fourier transform of cryo-electron microscopy imagery (**Figure 2a–c**) of both the *bchQRU* mutant and the wild-type chlorosomes, a layer line is visible, characteristic of *syn-anti* stacks with helical repeats (**Figure 2d**). This observation led to a structural model of BChl molecules that are self-assembled into coaxial cylinders to form tube-shaped elements with a lamellar spacing of $\sim$2.1 nm (**Figure 2e,f**). In *bchQRU* mutant chlorosomes the layer line is observed at 0.83 nm, revealing stacks running perpendicular to the tube axis and forming rings, whereas in wild-type chlorosomes the periodicity represented by a weak layer line at 1.22 ± 0.03 nm^{-1} corresponds to the distance between repeating *syn-anti* pairs in the direction of stacks running parallel to the tube axis (25).

The self-aggregated state of BChl *c* molecules in chlorosomes belonging to a *bchQ bchR* mutant, which mostly produces a single 17^2-farnesyl-*R*-[8-ethyl, 12-methyl] BChl *c* homolog, was characterized by the same integrated approach (24, 28). For this mutant a reproducible reflection at 1/0.69 nm^{-1} was observed with electron microscopy in the direction perpendicular to the curvature of cylindrical segments. In combination with distance information from NMR, this provided evidence for parallel stacking of BChl *c* molecules. In addition, a pronounced 1:1 doubling of selective ^{13}C and ^{1}H resonances in the solid-state NMR data revealed the presence of
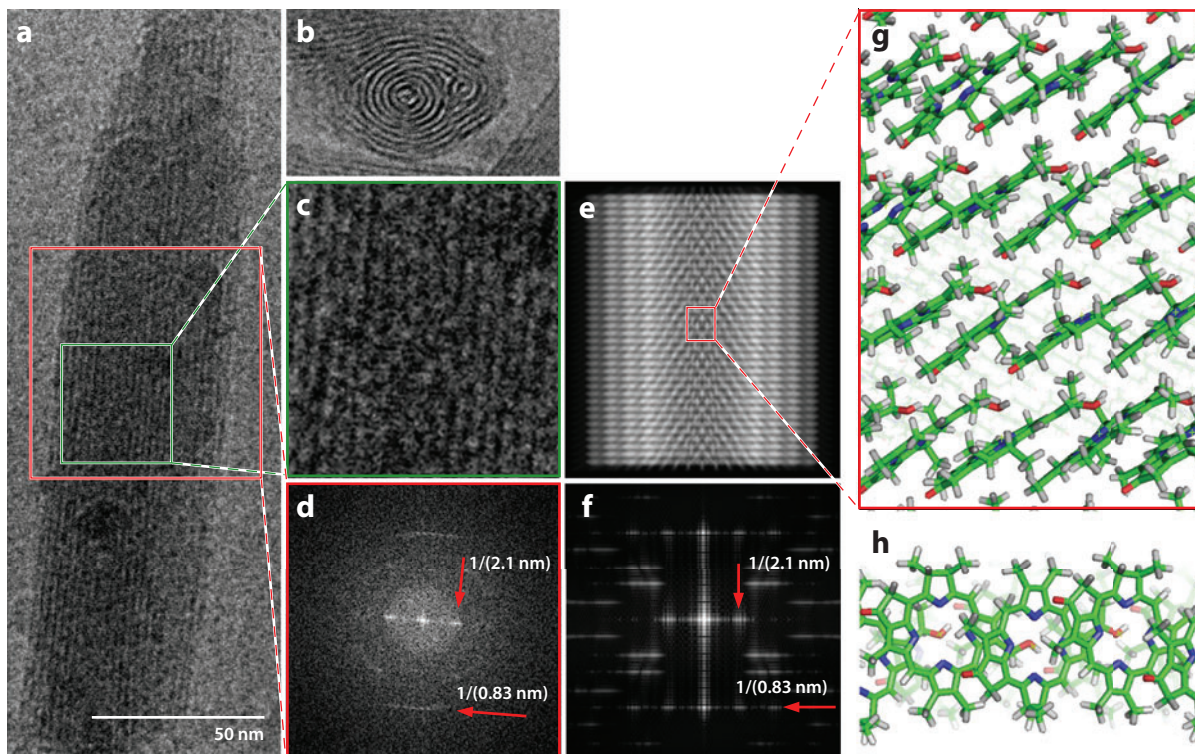
Figure 2

The chlorosome was the last photosynthetic antenna for which a detailed structure was not yet known, and recently the supramolecular organization of bacteriochlorophyll (BChl) *d* in very homogeneous chlorosomes of the *bchQRU* mutant of *Chlorobaculum tepidum* was resolved by computational integration of NMR data and cryo-electron microscopy (EM) images. (*a*) Side view of a chlorosome. (*b*) Top view of a chlorosome. (*c*) Enlarged view of panel *a*. (*d*) The Fourier transform of the red-boxed region in panel *a*, with reflections from a 2.1-nm spacing between BChl layers and a 0.83-nm spacing along the layers (*indicated by red arrows*). (*e*, *f*) The simulated EM image from a model comprising four tubes built from the NMR-derived and geometry-optimized structure shown in panels *g* (*side view*) and *h* (*top view*) for *syn-anti* monomer stacks of the 17^2-farnesyl-*R*-[8-ethyl, 12-methyl] BChl *d* that is synthesized by the *bchQRU* mutant of *C. tepidum*.

two distinct and nonequivalent BChl *c* components, attributed to microdomains of all *syn*- and all *anti*-coordinated parallel stacks. This finding led Ganapathy et al. (24) to propose that the heterogeneity in chlorosomes can be explained by phase separation and the formation of well-ordered domains of alternating stacking components with a correlation length of ∼40 monomers.

Perspectives on Common Denominators in the Biophysics and Evolution of Photosynthesis

The chlorosome template structures point to a bifunctional design, in which (*a*) quantum delocalization along stacks of BChl is facilitated by π–π overlap and tight packing, and (*b*) symmetry breaking of the lowest exciton state is favored by helical chains of activated hydrogen bonds between stacks. Upon excitation, a rotation of electric dipole moments that are aligned along the hydrogen-bond helix for high dielectric susceptibility and charge transfer bias promotes polaronic or charge-transfer character in the lowest exciton state (15, 60). This ferroelectric character

probably leads to a giant electric dipole moment that provides the basis for ultrafast, long-distance transmission of excitation energy by long-range Förster transfer all the way into the FMO (Fenna-Matthews-Olson protein) antenna complex (21, 52). The structural framework can accommodate chemical heterogeneity in the side chains for adaptive optimization of the light-harvesting functionality by optical tuning and broadening (25). In addition, the chlorophylls in chlorosomes form sheets that allow strong exciton overlap in two dimensions, enabling a self-protection mechanism where potentially damaging triplet excitons can encounter and annihilate for photoprotection (40).

The rotation of the electric dipole in a chlorin macrocycle affects the electronic structure and can shift the redox potential while keeping the optical transition energy essentially the same (44). This indicates a generic mechanism for shifting redox potentials, either by excitation or by shaping of the molecular structure. This is of interest for the biological design of water splitting by PSII, because the oxidation of H_2O is a multielectron process requiring the accumulation of four oxidizing equivalents at high redox potential, and the MAS NMR photo-CIDNP experiments on PSII have indicated that redox shifts of the chlorophyll dyes that do allow water splitting can be produced by local electronic structure effects from distortions induced by the protein (17, 44). Thus, although chlorosomes are very simple antennae built from self-assembled chlorophylls without a protein component, their biophysics is quite rich, with essential elements of exciton delocalization, of charge separation by proton-coupled electron transfer, and of redox tuning present in a strained structure, suitable for engineering by historically contingent evolution.

HISTIDINE-COFACTOR INTERACTIONS FOR LOWERING ENERGY BARRIERS IN PHOTOSYNTHETIC COMPLEXES

Imidazole side chains of His play a key role in biocatalytic molecular processes of proteins. Their imidazole side chains can occur in different protonation and charge states and can form hydrogen bonds. Interaction between His and the Mg^{2+} ion has been suggested for all BChl-protein complexes with known structures (16, 43, 59). Using MAS NMR studies in conjunction with site-directed isotope labeling, we (1, 3) have used histidines to probe the relation between the electronic structure and protein-induced stress in bacterial reaction centers (BRCs), as well as the light-harvesting antenna complex 2 (LH2), with the specific aim of resolving ground-state mechanisms for the activation of photosynthetic protein complexes for exciton and charge transfer.

Histidines in BRCs

The electronic environment of the special pair (P) and the balance of negative charge over the two halves ($P_L^{\delta-}$ and $P_M^{\varepsilon-}$) of the BRC of the purple bacteria *Rhodobacter sphaeroides* (**Figure 3a**) were probed by biosynthetic incorporation of His selectively isotope labeled at the imidazole side chain. MAS NMR data revealed an asymmetric electronic environment of P (3). Both ^{15}N and ^{13}C NMR data show two types of axial histidines, denoted Type 1_{axial} and Type 2_{axial} (**Figure 3d**). ^{15}N resonance data indicate that the τ nitrogens of three of the four axial histidines resonate at 225 ppm, while the fourth resonates at 220 ppm (**Figure 3b,c**). In the two-dimensional ^1H-^{13}C dipolar correlation spectrum of $[^{13}C_6,^{15}N_3]$-His-labeled RCs, the correlation signals from the axial histidines are resolved and well-separated from the response of the other histidines due to significant effects of the ring current on the axial histidines from the nearby chlorophyll macrocycles (**Figure 3e**). By integration of the ^1H-^{13}C cross-peaks, it was deduced that one axial histidine is different from the other three in the BRC (3). Thus, the ^{13}C data validate the observation by ^{15}N NMR of an axial histidine with a distinctly different electronic structure in the BRC.

BRC: bacterial reaction center

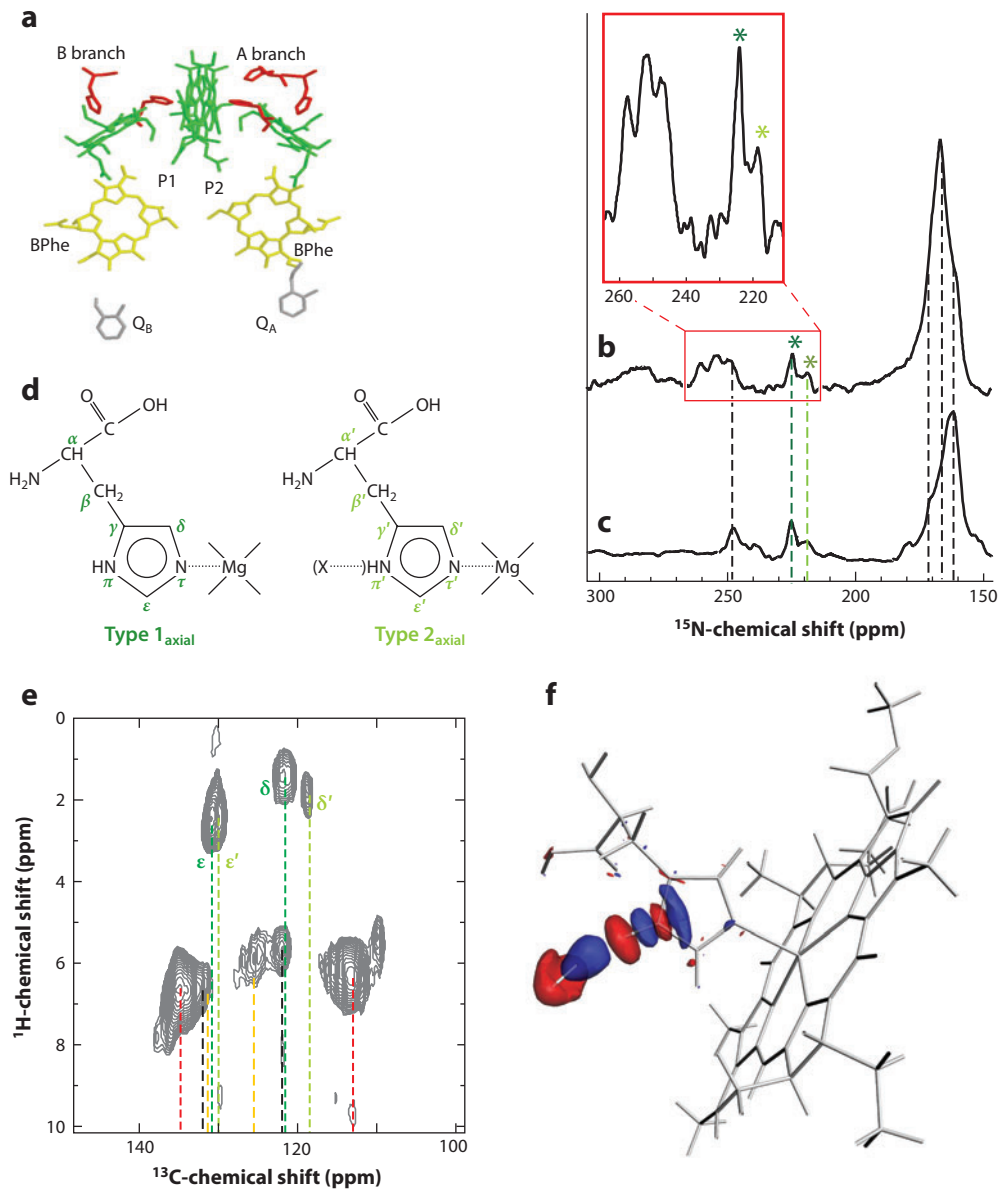**LH2:** light-harvesting antenna complex 2

Figure 3

For the bacterial RC, MAS NMR studies show that differential charge polarization of axial histidines balances symmetry breaking in the ground state of the special pair (P). (*a*) Arrangement of cofactors in RCs of *Rhodobacter sphaeroides* (R26). CP-MAS ^{15}N NMR spectra of (*b*) uniformly and (*c*) τ-^{15}N-His-labeled RCs. (*d*) The spectra reveal two different types of axial histidines, designated Type 1_{axial} (*dark-green dashed lines*) and Type 2_{axial} (*light-green dashed lines*), in bacterial RCs. (*e*) Contour plot sections of a 2D ^{1}H-^{13}C heteronuclear dipolar correlation spectrum of [^{13}C,^{15}N]-His-labeled bacterial RCs of *R. sphaeroides*. The significant effects of the ring current on the axial histidines caused their cross-peaks to separate from those of nonaxial histidines in the RC. (*f*) DFT calculations performed on BChl-His complexes with axially coordinated histidines and a hydrogen-bonded water molecule. The calculated electrostatic potential charges indicate a partial positive charge of +0.19 on the imidazole ring of this special axial His, which can be compared with the charge of +0.10 on the imidazole ring of an axial His that is not involved in hydrogen-bonding at its π nitrogen (3). Abbreviations: BPhe, bacteriopheophytin; MAS, magic-angle spinning; RC, reaction center; DFT, density functional theory; BChl, bacteriochlorophyll.

Histidines in LH2

Light-harvesting antenna complex 2 (LH2) is a peripheral antenna complex that absorbs light and transfers the excited state energy to the LH1-RC complex. A high-resolution X-ray structure of the LH2 of *Rhodopseudomonas acidophila* showed remarkable symmetry in the arrangement of light-absorbing pigments in its protein matrix (12, 46). The whole complex is an oligomer of nine identical units arranged in a ring (**Figure 4a**). Each unit consists of a pair of small hydrophobic apoproteins (named α and β), a pair of BChl *a* molecules absorbing at 850 nm (B850), and one BChl *a* molecule absorbing at 800 nm (B800). The 18 B850 molecules form a closely interacting ring. Going around the ring of B850 molecules, the Mg^{2+} ions are coordinated alternately to the His30 on the β apoprotein (β-His30) and to His31 on the α apoprotein (α-His31) (**Figure 4b**). These two histidines are highly conserved in different bacteria. This overall assembly of the B850 ring acts as an energy storage device, preserving excitation energy until it is forwarded to other rings and ultimately to the BRC (5, 33, 50).

Both Type 1 (neutral) and Type 2 (positively charged) histidine residues are resolved in the MAS NMR data collected for LH2 (3) (**Figure 4c**). By using two-dimensional heteronuclear (^{1}H-^{13}C) dipolar correlation spectroscopy, a clear and unambiguous assignment of the protons of histidine interacting with the magnesium of a BChl *a* molecule in LH2 is obtained and a significant ring current effect of BChl B850 on the coordinating histidine is resolved (**Figure 4d**). Using the ring current shift on ^{1}H, we clearly distinguish the electronic structure of coordinating histidines from positively charged histidines in LH2. The results from MAS NMR can be used in the next step of density functional theory (DFT) analyses to resolve protein-induced geometric constraints on the Mg-coordinated histidine in LH2 (see Structural Frustration and Activation: The Role of Molecular Modeling, below). Finally, the NMR data indicate that the ground-state electronic structures of individual BChl *a*–His complexes are largely independent of supermolecular π interactions in the assembly of a ring of 18 B850 molecules in LH2.

ELECTRONIC STRUCTURE OF THE DONOR

The solid-state photo-CIDNP effect, discovered by Zysmilich & McDermott in 1994 (78), allows the signal enhancement of tens of thousands of factors for ^{13}C MAS NMR in a magnetic field of 4.7 T (200 MHz ^{1}H frequency) for BRCs in wild-type and the carotenoid-less mutant R26 of *R. sphaeroides* (57, 58, 69). Such strong signal enhancement has enabled researchers to observe select radical pairs at nanomolar concentrations (34, 58). Owing to the long relaxation time of ^{13}C in solids, nuclear polarization of subsequent photocycles can be accumulated in continuous illumination experiments, making photo-CIDNP MAS NMR a sensitive analytical tool for studying radical pairs (17, 65, 66). The effect has been observed in all natural photosynthetic RCs studied so far (45).

Photo-CIDNP Studies of Electron Transfer Mechanisms in the BRC

The spin-chemical processes associated with the kinetic stabilization of intermediates in the photocycle are indicated in **Figure 5a** (31, 69). When illuminated, BRCs form radical pairs. The radical pair is formed by a radical cation at the two donor BChls that form the special pair P, and by a radical anion on the bacteriopheophytin acceptor cofactor (Φ) of the active branch. The radical pair mechanism (RPM), well established in liquid-state photo-CIDNP, is active in spin-sorting (i.e., enriching one nuclear spin state in one of the two decay channels of the radical pair and depleting it in the other) (11, 39). Because the product states of both branches of the radical-pair decay channels are

Density functional theory (DFT): a quantum mechanical modeling method applied here to investigate the structure and chemical bonding of molecular motifs involved in photosynthetic energy conversion
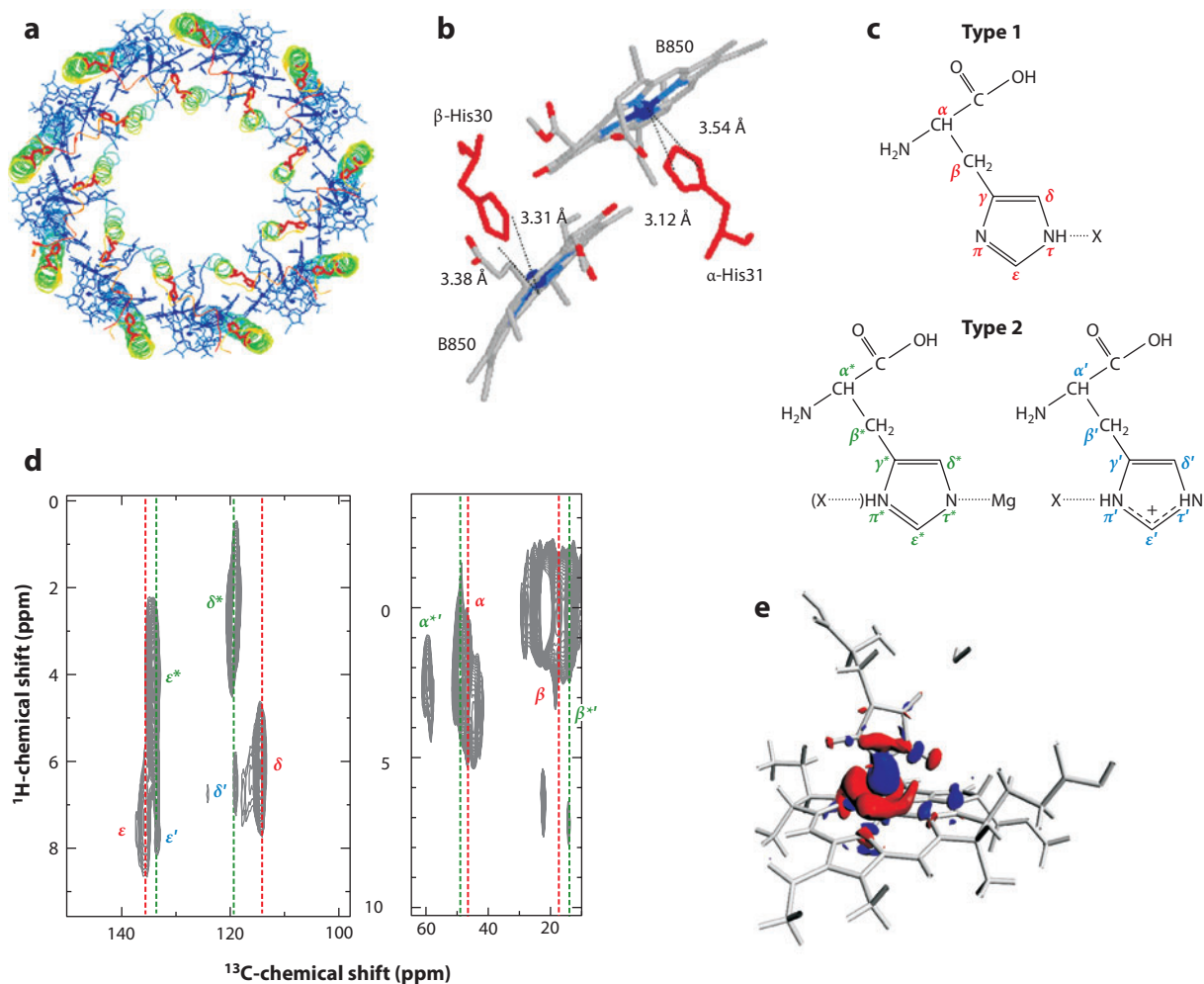
RPM: radical pair mechanism

Figure 4

For LH2, MAS NMR spectroscopy provides access to the electronic structure of coordinated histidines and enables an assessment of charge transfer to the BChl and electronic delocalization effects. (*a*) Top view of the LH2 of *Rhodopseudomonas acidophila* showing the arrangement of histidines (*red*). (*b*) A section of the LH2 ring showing the distances between the δ and ε carbons of β-His30 and α-His31, and the central Mg^{2+} ions of coordinated B850 molecules. The aliphatic chains of the BChl have been omitted for clarity. (*c*) Two types of histidine residues were resolved: Type 1 (neutral) and Type 2 (positively charged) (2). (*d*) 2D heteronuclear (^{1}H-^{13}C) dipolar correlation spectrum of [^{13}C$_6$,^{15}N$_3$]-histidine-labeled LH2 complexes collected in a field of 17.6 T. (*e*) Change in the electronic density upon BChl-His complex formation calculated by DFT. The isosurface value is 0.0012 e/Å^3. Red indicates an increase in the electron density in the complex, compared to the separated BChl and His fragments; blue denotes a decrease in the electronic density. These DFT results for the BChl *a*–histidine complexes in LH2 provide evidence that the protein environment stabilizes the histidine close to the Mg^{2+} ion, thereby inducing a considerable charge transfer of ∼0.5 e. Owing to this protein-induced geometric constraint, the Mg-coordinated histidine in LH2 appears to be in a frustrated state very different from the formal neutral$_π$ form, which is consistent with the NMR chemical shift data (1, 73). Abbreviations: LH2, light-harvesting antenna complex 2; MAS, magic-angle spinning; BChl, bacteriochlorophyll; DFT, density functional theory.

identical, time-resolved experiments are required to observe spin-sorting by the RPM (**Figure 5b**). The initial positive (absorptive) transient RPM polarization is visible up to 10 μs, because the nuclear polarization occurring on the triplet decay pathway is shifted and broadened beyond detection by the nearby paramagnetic carotenoid triplet (74). After the decay of the RPM-type response, another pattern on the 100 μs timescale emerges with a negative (emissive) envelope. This is due to the solid-state mechanisms three-spin mixing (TSM) (35, 36) and differential decay (55). These mechanisms transfer the initial electron spin zero-quantum coherence, which is created upon the generation of the radical pair in the S state in the S-T_0 manifold of states, into net nuclear polarization. In the electron-electron nuclear TSM mechanism, the symmetry of the coherent spin evolution in the correlated radical pair is broken by state mixing due to electron-electron coupling, nuclear Zeeman interaction, and pseudosecular hyperfine coupling. State mixing is maximized for a double matching of the difference of the electron Zeeman frequencies $\Delta\Omega$, the nuclear Zeeman frequency ω_I, and the secular part of the hyperfine interaction A, according to $2|\Delta\Omega| = 2|\omega_I| = |A|$. In the differential decay mechanism, the symmetry between the singlet and triplet decay pathways is broken by different lifetimes of the S and T_0 states of the radical pair and by pseudosecular hyperfine coupling. In this case, only a single matching of interactions $2|\omega_I| = |A|$ is required, and the difference of singlet and triplet radical pair lifetimes should be of the order of the inverse hyperfine coupling.

Solid-state photo-CIDNP NMR experiments provide a wealth of information on the radical pair. Here we focus on the findings for two electronic structures of the special pair (P).

1. The chemical shifts of the cofactor nuclei can be obtained selectively, even for large systems. In **Figure 5c**, A and A′, the chemical shifts of P_L and P_M, are expressed relative to the shifts for monomeric BChl *a* in acetone. The figure shows the relative electron densities for a sample in the dark after the photocycle. These data nicely illustrate that the P_L deviates more from the monomer than the P_M does. In addition, both cofactors show enriched electron density in the overlap region of the two BChls, confirming the special pair (P) supermolecule arrangement for the BRC donor.

2. Time-resolved photo-CIDNP MAS NMR allows for the observation of RPM-based transient nuclear polarization, which is related to the isotropic hyperfine interaction a_{iso} (**Figure 5c**, B and B′) and depends on local electron spin densities (14). In contrast to the ground state, the radical cation does not concentrate unpaired electron spin density in the overlap region. Because both the ground-state electron density and the radical-cation electron spin density refer to the same molecular orbital, this difference points to symmetry breaking of P in the photochemistry (see Structural Frustration and Activation: The Role of Molecular Modeling, below). In **Figure 5c** (C and C′), the a_{iso} is calculated for the two cofactors and the axial histidines. A good correspondence between theory and experimental data strongly suggests that the functional properties of P are determined largely by shaping and that, for example, electrostatic tuning by the surrounding matrix may be less important.

Electronic Structure of the Primary Donor in Plant PSII

Figure 6a shows the donor Chl *a* cofactor with the intensities of the steady-state photo-CIDNP MAS NMR signals. These signals are from solid-state mechanisms and reflect the local p_z electron spin density (17). Three light-induced ^{15}N signals reveal a pronounced asymmetry of electron spin density, which appears to be shifted toward pyrrole ring IV of the donor Chl *a* (17). ^{13}C photo-CIDNP MAS NMR data indicate maximum electron spin density at the C-15 methine carbon adjacent to ring IV (44). The electron spin density pattern for the donor cofactor of PSII appears

TSM: three-spin mixing

inverted compared to the donor and acceptor cofactors of PSI and monomeric Chl *a* in solution (17).

Additional light-induced ^{15}N and ^{13}C signals in PSII have been assigned to a Type 1 His. A ^{15}N signal was attributed to the nitrogen N-π, and three emissive signals at 142.5, 139.8, and 129.2 ppm represent the ^{13}C side chain response (2). All four signals assigned to the His are significantly broader than the donor signals. A reduction in spin density was observed by EPR and originally interpreted in terms of a weakly coupled dimer, with ~82% of the spin density on one Chl cofactor (62). According to the MAS NMR data, a distribution of electron spin density over both the donor Chl and its axial histidine is more likely. Because the two accessory chlorophylls Chl_{D1} and Chl_{D2} are not coordinated to histidines (20, 77), the MAS NMR data contribute to converging evidence that the donor is either P_{D1} or P_{D2} (37, 41, 76).

For a Type 1 histidine with a deprotonated π-position, the donor in the electronic ground state would be a [Chl His] complex with excess negative charge, and in the photo-oxidized state it would be a neutral radical. We have proposed a hinge-type model for the donor complex that
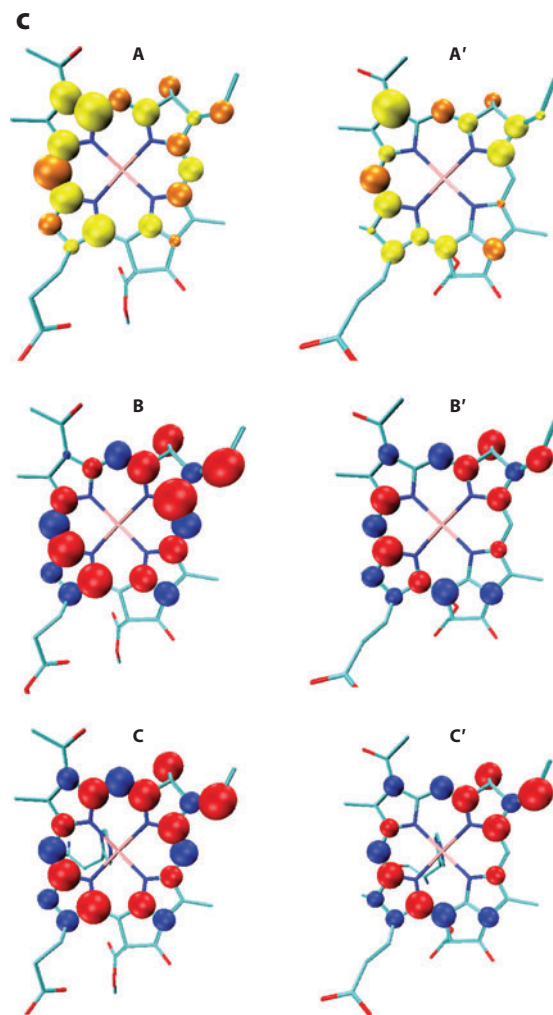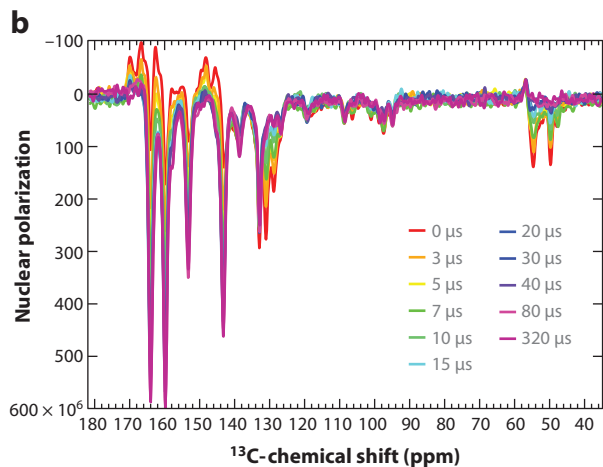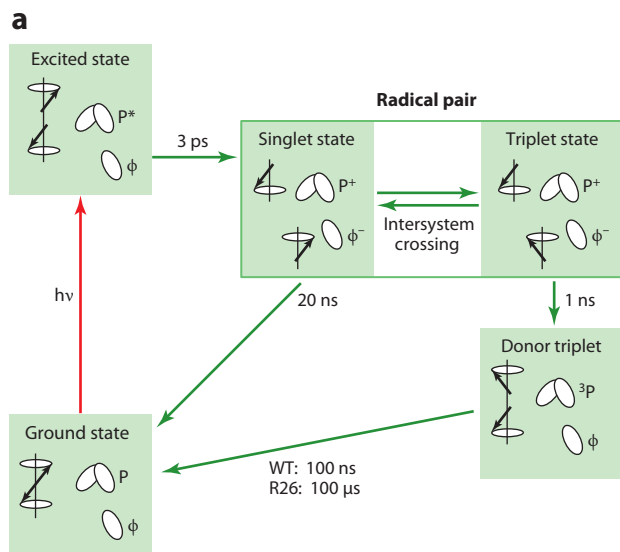
unifies those aspects (17) (**Figure 6b**). Minor bending of the axial histidine toward pyrrole ring IV and the methine bridge C-15 leads to a π-π overlap of both conjugated systems, modulates the Chl-His distance, and stabilizes a negatively charged electronic ground state of the complex at a high redox potential required for water oxidation.

STRUCTURAL FRUSTRATION AND ACTIVATION: THE ROLE OF MOLECULAR MODELING

Molecular modeling plays an increasingly important role in complementing experimental findings and supporting the interpretation of the data. In particular, DFT in combination with molecular dynamics simulations is a powerful and efficient computational tool that bridges various experimental approaches and resolves complex mechanisms of function in photosynthetic antennae and RCs (9). Quantum-mechanical calculations are especially important for elucidating the link between structure and mechanisms of function in these molecular complexes and for investigating at the atomic level the key mechanisms developed by nature during evolution. We use a combination of different approaches with different levels of approximation as well as the available experimental structural data to determine and apply evidence-based constraints, often in the form of structural constraints, to the buildup of the model.

BChl-His Complexes in LH2

In the BChl-His motifs that support the conversion of solar energy to chemically useful compounds in a wide range of photosynthesis processes, the histidine imidazole side chain is physically frustrated between the aromatic and conjugated electronic states, which makes it easy for the biological environment to gain control over the chemical structure. Because the histidine can undergo tautomeric changes and is able to form hydrogen bonds, it can act as both proton donor and proton acceptor and thus can play the role of mediator in proton transfer processes. Four different protonation forms of the imidazole ring are possible: a formally anionic imidazolate form, either of two

←——

Figure 5

(*a*) Photocycle and kinetic stabilization of intermediates for photo-CIDNP in quinone-blocked RCs of *Rhodobacter sphaeroides* WT and R26. The cofactor arrangement is identical to that shown in **Figure 3a**. Upon illumination and fast electron transfer from an excited singlet state, a radical pair is formed in a pure singlet state. The radical pair is formed by a radical cation at the two donor BChls that form the special pair P, and by a radical anion on the BPhe acceptor cofactor (Φ) of the active branch. The chemical fate of the radical pair depends on its electronic spin state: The singlet state is allowed to recombine, whereas for the triplet state direct recombination is forbidden, and a donor triplet (^{3}P) is formed by intersystem crossing. The lifetime of ^{3}P depends on the relaxation channels provided by the environment. Therefore, the lifetime is short in WT RCs that have a carotenoid at a short distance from the donor, and significantly longer in the carotenoid-less mutant R26. (*b*) Time-resolved photo-CIDNP ^{13}C MAS NMR spectra of 4-ALA-labeled RCs of WT *R. sphaeroides* obtained with delay times from 0 to 320 μs. The initial transients (*red-orange*) are the positive signals originating from a RPM contribution, while the later transients (*blue-lilac*) are due to the solid-state mechanisms TSM and DD. (*c*) Electronic structures of the primary donor P of *R. sphaeroides*. The chlorophylls of P_L (*left*) and P_M (*right*) depicted in **Figure 3a** have different electron densities on the macrocycle that can be determined from the photo-CIDNP data. (A and A′) Electron densities of P_L and P_M in the electronic ground state derived from chemical shift differences are relative to the shifts for monomeric chlorophyll in acetone in consideration of ring current effects. (B and B′) ^{13}C electron spin densities on P_L and P_M obtained experimentally from RPM intensities observed at zero delay between light excitation and NMR detection. (C and C′) Normalized local isotropic hyperfine interaction a_{iso} for the ^{13}C in P_L and P_M derived from DFT computations, with P_L and P_M coordinated to His L173 and His M202, respectively. To visually compare the experimental data with theory, both data sets were normalized using the cumulative volume of the red and blue spheres (14). Abbreviations: CIDNP, chemically induced nuclear polarization; RC, reaction center; WT, wild type; BChl, bacteriochlorophyll; BPhe, bacteriopheophytin; MAS, magic-angle spinning; RPM, radical pair mechanism; TSM, three-spin mixing; DD, differential decay.
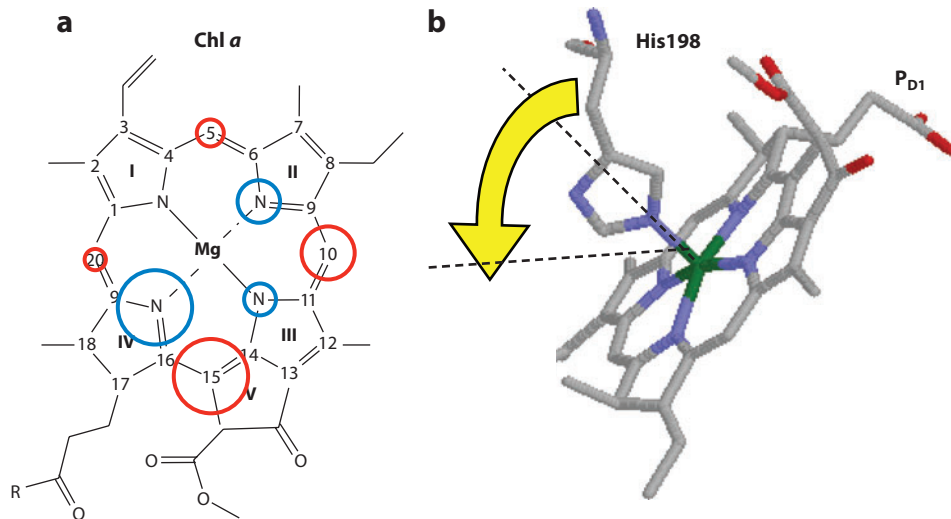
Figure 6

(*a*) Based on the ^{13}C (*red circles*) and ^{15}N (*blue circles*) photo-CIDNP intensities, the electron spin density pattern for the donor cofactor of plant photosystem II is shown. The size of the circles is relative to the intensity of the signal. (*b*) The hinge model of the electron donor in photosystem II. Owing to the tilt of the axial histidine toward pyrrole ring IV (*indicated by the arrow*), the electron spin density pattern is inverted relative to monomeric Chl and is partially on the axial histidine. Abbreviation: CIDNP, chemically induced nuclear polarization.

neutral tautomers (N_π-H or N_τ-H) depending on which nitrogen in the ring is protonated, and a doubly protonated (positive) imidazolium form. Because the reactivity involves the nitrogen atoms in the imidazole ring, biochemical mechanisms involving the His can be resolved when the protonation states are determined by quantum chemical calculations of chemical shifts in combination with NMR spectra. We have demonstrated the viability of this concept for LH2 (72).

Solid-state NMR data have shown that the five histidines in LH2 can be classified as either Type 1 or Type 2 on the basis of their chemical shifts. Type 1 includes α-His37 and β-His12 and corresponds to neutral N_τ-H histidines (1, 2). The α-His31, β-His30, and β-His 41 are Type 2 and have a ^{13}C chemical shift pattern corresponding to positively charged histidines. However, while the β-His41 has both nitrogens in the ring protonated, the α-His31 and β-His30 are coordinated by the N_τ to the Mg^{2+} ion of the BChl *a* molecules. Therefore, the α-His31 and β-His30 are formally neutral N_π-H tautomers, which is consistent with the experimental anisotropy parameters for N_τ that indicate a pyridine-like $\geq N|$ electron configuration, with a nonbonding lone pair at the nitrogen. This finding contrasts with the experimental observation of ^{13}C chemical shifts for the Mg-coordinated histidines matching those of the positive β-His41, with a $>$N-H pyrrole configuration for both nitrogens and the lone pairs contributing to the aromaticity of the imidazolium side chain.

DFT shift calculations performed on a BChl-His complex extracted from one of the B850 BChl dimer units of the LH2 crystallographic structure of *Rhodopseudomonas acidophila* clarify this apparent inconsistency. The results show that the DFT ^{13}C chemical shifts are in much better agreement with the experimental values when the X-ray structure is considered without performing a geometry optimization. The main effect of the geometry optimization is to increase the N_τ-Mg distance

and to rotate the imidazole ring plane around the Mg-N_τ axis. These changes in the geometry correspond to a change in the total charge of the histidine, which is considerably more positively charged in the crystallographic structure, thus clarifying why the neutral Mg-coordinated histidine behaves as a positive histidine according to the ^{13}C NMR data.

The main conclusion is that the constraints due to the protein environment have a significant effect on the electronic structure of the BChl-His complex and lead to a large charge transfer of $\sim$0.5 e (**Figure 4e**). The Mg-coordinated histidines can be described as being in an anomalous state of physical frustration very different from the neutral N_π-H form. Although the ^{13}C data show the character of a positively charged histidine, the Mg-coordinated N_τ still maintains its pyridine character. This is confirmed by the calculated anisotropy parameters for N_τ in the BChl-His complex, which match the shift anisotropy expected for pyridine-type nitrogens and confirm a state of frustration, particularly for N_τ.

The concepts of localized strain and misfits induced by the protein folding are important for the foundation of basic functional mechanisms involved in tuning the electronic properties and exciton coupling in LH2. For instance, the protein-induced charge transfer in the BChl-His complex can affect the absorption spectra of the B850 BChls and the excitation energy transfer processes in LH2 (70). In addition to the excitation site energies and transition dipole moments of the BChl-His complex, the long-range electrostatic interactions with the protein environment may be affected significantly.

NMR Secondary Shifts in LH2 Antennae

Protein NMR secondary chemical shifts are widely used to predict the secondary structure, and in solid-state NMR, they are often the only unambiguous structural parameters available (75). However, the employed prediction methods are empirical, relying on the assumption that secondary shifts are only affected by shielding effects from neighboring atoms. This contrasts with the nature of chemical bonding and structure in photosynthetic membrane proteins, which are very tightly packed with a high density of cofactors and form complex chemical topologies to reach their final shapes and biological activity. With solid-state NMR, a sequence-specific assignment of the ^{13}C and ^{15}N responses of the transmembrane helix regions of the LH2 of *Rps. acidophila* was obtained (**Figure 7**). The secondary shifts were determined and compared with chemical shifts predicted from the available X-ray structure (PDB ID: 1NKZ) using SHIFTX (54). This program uses a semiempirical approach to estimate shifts for a PDB structure from a database of NMR shifts, and calculates the contributions of electrostatic side chains, hydrogen bonding, and ring current to the chemical shift (48).

For the densely packed LH2, several residues exhibit pronounced secondary shift anomalies, and the majority of these residues are involved in pigment-protein or protein-protein contacts (**Figure 7**). DFT shift calculations confirm that the backbone chemical shifts are sensitive to higher-order contacts in the quaternary structure that induce atomic-level structural or electronic perturbations. The residues exhibiting pronounced shift anomalies include the BChl-coordinating histidines α-His31 and β-His30 and a phenylalanine (αF41) that has strongly twisted C_β-C_α-C and C_α-C-N conformations in the LH2 crystal structure (54). Hence, although protein-induced structural distortions and electronic perturbations of the cofactors in photosynthetic antennae affect and control the excited-state energies, the DFT analyses of secondary shifts show that the interactions between the protein matrix and the cofactors are mutual, because the protein environment is also perturbed. This provides a complementary view of functional molecular interactions in natural light-harvesting assemblies.
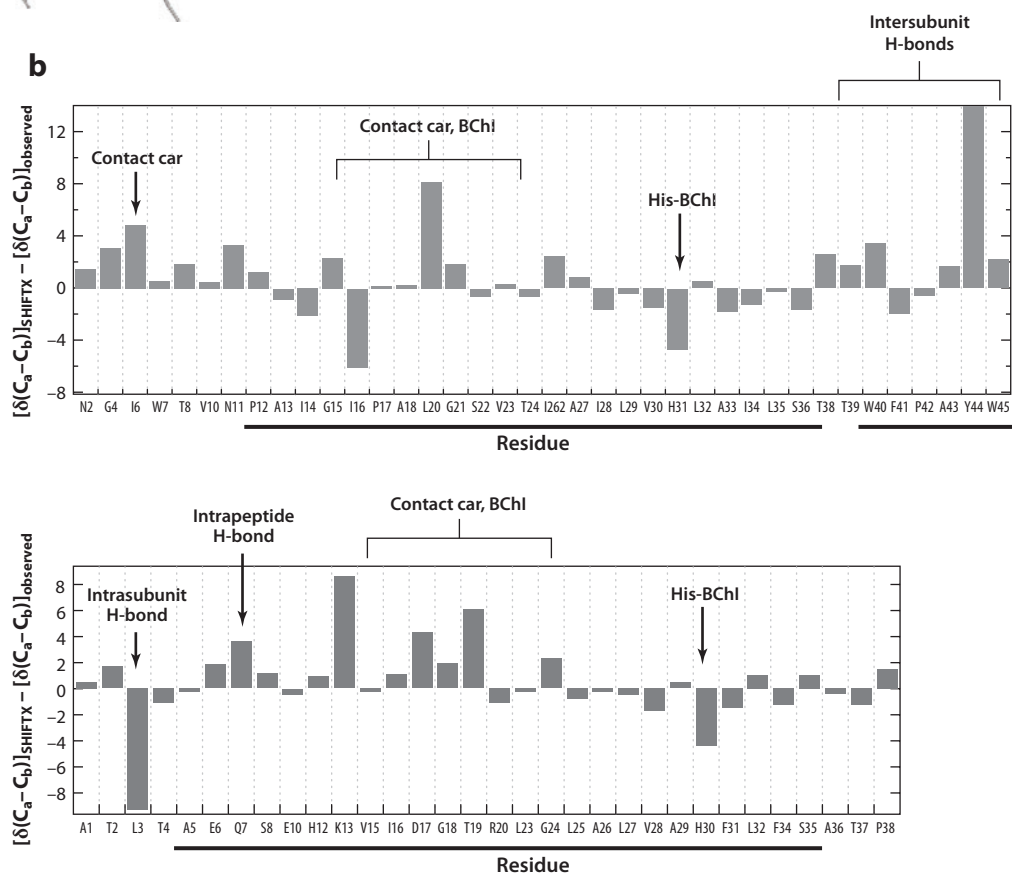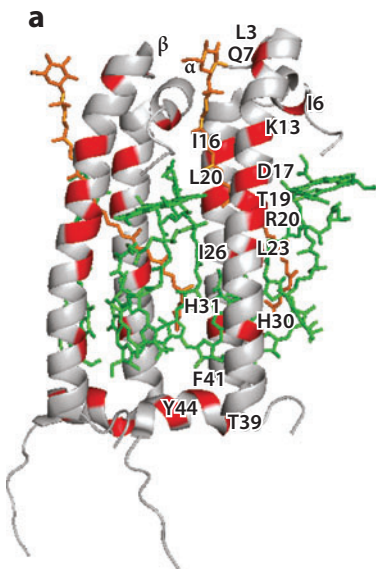
Symmetry Breaking and Dynamics for Unidirectional Charge Separation in BRCs

An important step in photosynthesis is the photo-induced charge separation in RCs. A detailed understanding of this process will likely provide essential information for the development of biomimetic devices for artificial photosynthesis. X-ray structures have revealed that BRCs resemble PSII of higher plants, with the L- and M-polypeptides and associated cofactors arranged in two nearly symmetric membrane-spanning branches (16, 19, 68). Despite an apparent structural symmetry of the RC, spectroscopic studies have shown that only one of the two potential electron transfer chains, the L-branch, is active in catalyzing the electron transfer (29). Electronic asymmetry in the special pair (P) of the BRC is thought to influence the directionality of the electron transfer process and has been studied extensively (4, 38). The photo-CIDNP solid-state NMR experiments discussed above have revealed electronic asymmetry, both for the electronic ground state and for the radical cation state (14). The specific role of the protein environment in the initiation of electron transfer and a precise indication of how P is activated by the neighboring residues for charge separation were studied with quantum-mechanical modeling tools (18).

One thoroughly investigated aspect was the possibly active role of the histidines in the BRC. DFT prediction of chemical shifts combined with solid-state NMR data led Alia et al. (3) to assign protonation states and interpret the NMR response of the 4 Mg-coordinated histidines and the other 12 histidines in the BRC. It was established that all four axial BChl a–ligating histidines exist in the neutral N_π form. The electronic structure of one His is different from that of the other three, which is attributed to the presence of a hydrogen-bonded water at the N_π nitrogen of the special His that breaks the apparent structural symmetry for the four axial histidines in the BRC. According to the DFT calculations, the hydrogen bond interaction reorganizes the electron density within the imidazole ring. This reorganization leads to a shorter distance between the histidine and BChl a and to a larger donation of electrons from the histidine to the BChl a than from the other three coordinating histidines (**Figure 3f**). Thus, protein folding appears to impose a local conformation that induces a special electronic structure and hydrogen-bonding environment for a coordinating histidine.

The X-ray data of the *Rhodobacter sphaeroides* R26 (PDB ID: 2HJ6) indicate that His L173 is ~0.2 Å closer to the Mg compared to His M202 (64). Therefore, His L173 was thought to be the special histidine, although no direct evidence was available (3). To further explore this issue, DFT calculations have been performed on an extended model extracted from the 1PCR crystal structure of *R. sphaeroides*, including P, the two axial histidines (His L173 and His M202); two water molecules (HOH 1007 on the L-side and HOH 1051 on the M-side); and the amino acid residues His L168, Asn L166, and Phe M197 (73). The geometry of the model was partially optimized by relaxing the atomic positions of the imidazole ring, the Mg^{2+} ion, and the two hydrogens of

← ——

Figure 7

(*a*) Two subunits in the structure of the LH2 *Rhodopseudomonas acidophila* complex, highlighting the residues with experimental secondary shifts deviating >4 ppm from the SHIFTX-estimated values or with large individual δCO, δC$_a$, or δC$_b$ chemical shift displacements >4 ppm for the αβ subunit (*right*). (*b*) Difference shifts between the experimentally observed and SHIFTX-predicted secondary shifts defined as $\delta_{\text{SHIFTX-obs}} = [\delta(C_a - C_b)]_{\text{SHIFTX}} - [\delta(C_a - C_b)]_{\text{observed}}$ for the (*top*) LH2 α and (*bottom*) LH2 β polypeptides. The α-helical parts of the protein sequences are underlined. Cofactor-protein or protein-protein contacts coincide with anomalous shift regions, and the highlighted residues are involved in intrasubunit H-bonds, van der Waals contacts with the carotenoids and B800 BChl cofactors, and His coordination with the B850 BChl and intersubunit H-bonds. Abbreviations: LH2, light-harvesting antenna complex 2; H-bond, hydrogen bond; BChl, bacteriochlorophyll.

the water molecule while keeping all the other atomic coordinates fixed to the crystallographic data. These structural constraints were introduced to maintain the geometric shape of the complex induced by the protein environment. It was found that both axial histidines donate electron charge to P and that the inclusion of water molecules hydrogen-bonded to the axial histidines enhances the charge transfer for the P_M half of P. The calculated electrostatic potential charges indicate a partial positive charge of +0.19 on the imidazole ring of the special axial His, a positive charge of +0.10 on the imidazole ring of axial His that is not involved in hydrogen-bonding at its π nitrogen, and a net negative charge on P. A $P_L^{\delta-} P_M^{\varepsilon-}$ charge-transfer character and associated symmetry breaking of the electronic structure can trigger asymmetric electron transfer following excitation and can explain the different ^{13}C chemical shifts observed with photo-CIDNP (14, 67).

A hydrogen bond between the water and the first electron acceptor B_A might dynamically stabilize the oxidized special pair $P^{\bullet+}$, thereby facilitating electron transfer from P^* to B_A. Transient spectroscopy data have shown that the water molecule forming a hydrogen-bond bridge between His M202 and B_A is important for the optimization of the primary electron transfer rate (56). Hence, our theoretical results as well as experimental observations point to the special status of what are most likely His M202 and its coordinated water molecule in the transfer path. The existence of this effective proton-coupled electron transfer channel is currently being investigated.

Another symmetry-breaking feature of the protein environment of P is the presence of the histidine His L168 that is hydrogen-bonded to the 3^1 acetyl group of P_L. His L168 can play a role in tuning the electronic and optical properties of P. Its hydrogen bond can determine the orientation of the 3^1 acetyl group that is conjugated to the π electron system of BChl a. The conjugation decreases in strength as the carbonyl group is rotated out of the macrocycle plane, and by enforcing conformational changes to the acetyl, the protein can tune the biophysical properties of P (73).

Although a static computational approach can provide much useful information, dynamics cannot be neglected for a realistic description of the charge separation process, as low-frequency collective modes of P effectively remove the barrier for charge separation in photosynthetic bacteria along selective reaction coordinates (18, 49). Ab initio molecular dynamics simulations constitute an ideal computational tool to directly observe how the dynamic evolution of the nuclear coordinates is coupled to the corresponding electronic structure rearrangement calculated with DFT. We have recently reported such simulations at room temperature, both in the ground state and excited state, for a model including the BRC special pair and the relevant closest protein environment (18).

The ground-state trajectories reveal a dynamic localization of frontier orbitals (HOMO-LUMO) that is characteristic of P at room temperature. On a timescale of ~ 1 ps the HOMO (highest occupied molecular orbital) fluctuates and changes from complete localization on one dimer half to intermediate delocalization to complete localization on the other dimer half. The LUMO (lowest unoccupied molecular orbital) shows the same dynamics with opposite phase: When the HOMO is localized on P_M the LUMO is localized on P_L, and vice versa. This ground-state thermal fluctuation of electron density over P is linked to the tuning of the orbital energy levels by coupling with collective low-frequency vibrational modes. In particular, we identify a normal mode at ~ 50 cm^{-1} with a large projection on the hydrogen bond, with His L168 showing a strong dynamic correlation with the P_L HOMO energy (see **Supplemental Movie 1**, follow the **Supplemental Material link** from the Annual Reviews home page at **http://www.annualreviews.org**). After electronic excitation, we demonstrate how a specific mode at ~ 100 cm^{-1} couples to P^*, representing the reaction coordinate along which the excited state develops. We suggest that this mode was observed in resonance Raman studies (96 cm^{-1}) (10), in femtosecond absorption spectroscopy (94 cm^{-1}) (63), and possibly in hole-burning investigations (~ 150 cm^{-1}) (61).
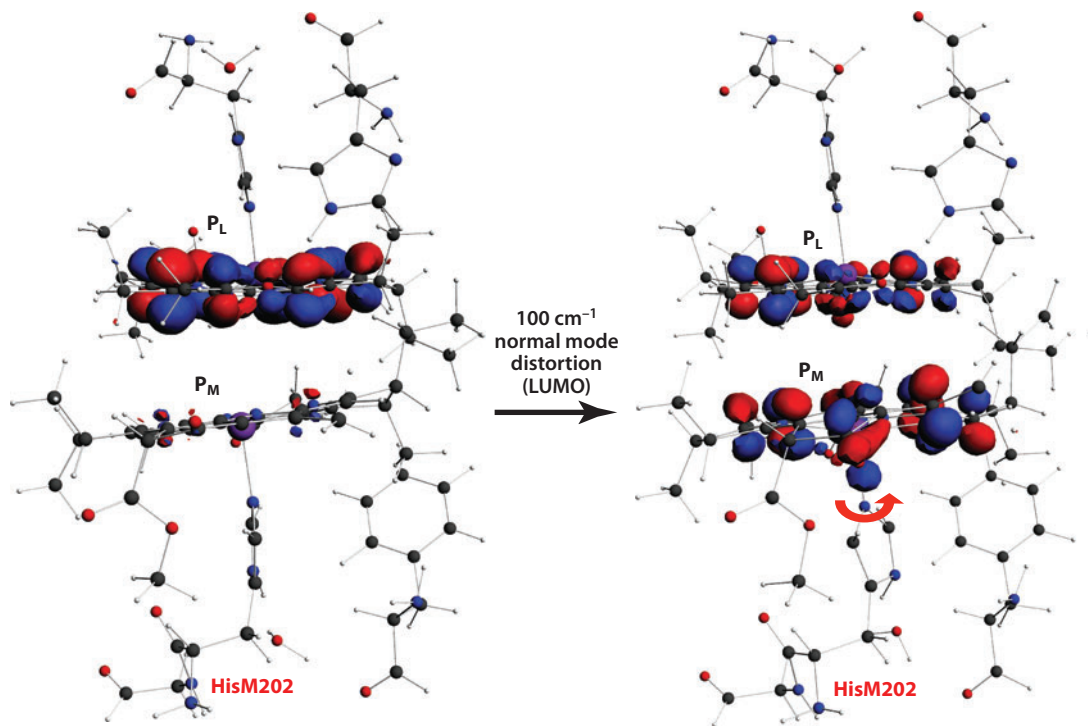
Figure 8

Dynamic symmetry breaking for enhanced charge-transfer character in the primary donor of the photosynthetic bacterial reaction center. The figure shows the LUMO redistribution for a displacement along the 100 cm^{-1} normal coordinate corresponding with a rotation of the His M202 around the coordination Mg-N$_\tau$ axis from 5° (*left*) to 50° (*right*). Abbreviation: LUMO, lowest unoccupied molecular orbital.

The predicted characteristic vibrational coordinate is the rotation of an axial histidine (His M202), which selectively lowers the energy of one (P$_M$) of the two BChls of P. This leads to symmetry breaking from a unidirectional displacement of electron density to establish an excited state with strong P$_L^+$P$_M^-$ charge-transfer character, a conclusion that is well supported by an extensive framework of experimental evidence (47).

To illustrate excited-state electron density redistribution due to the coupling of the excited state with the 100 cm^{-1} collective vibration, we show in **Figure 8** how the LUMO is affected by a displacement along this normal mode. The amplitude of the displacement is chosen such that the His M202 dihedral angle, representative of the rotation of the histidine around the coordinating Mg-N$_\tau$ axis, increases from 5° to 50°. This confirms that the reaction coordinate, even when starting from a P$_L^-$P$_M^+$ charge transfer configuration, leads to a P$_L^+$P$_M^-$ intermediate state through the coupling of P* to the 100 cm^{-1} mode, thus increasing the dihedral angle and initiating a directional displacement of electron density.

The charge displacement during the motion along the normal coordinate in the excited state proceeds against the background of many other vibrations, and its activation for efficient and enhanced electron tunneling is encoded by the biological design of the ground-state chemical topology of the BRC responsive matrix environment of P. In essence, the coupling between the electronic excitation and the specific vibrational modes facilitates the electrons tunneling through a barrier, making the charge-separated product state accessible from the reactant. This

Chemical topology:
method in which biological molecular motifs can reach their final shape and achieve their reactivity

may represent a general principle for the chemical design of bio-inspired molecular rectifiers that mimic the classically coherent dynamics of P (see **Supplemental Movie 1**).

BIO-INSPIRED NANOMACHINES: FROM BIOPHYSICS TO ARTIFICIAL DEVICES

Many scientists believe that it will be possible to apply the principles of light harvesting, charge separation, and multielectron catalysis in photosynthesis to the chemical design and synthesis of responsive matrices for the production of hydrogen- or carbon-based solar fuel on a large scale, using water and CO_2 as raw materials (53). Natural photosynthesis converts the equivalent of 100–200 TW of power, which is about ten times more than the ~14 TW that is currently dissipated by our economies. Photosynthesis is an energy source with a proven ability to perform geo-engineering in a sustainable manner, in the sense that it is fully integrated into the biological hierarchy at every scale and can be drawn upon by biology for evolution and development. Evidence is accumulating for nonreversible anthropogenic changes, and merging human activity with the ecosystem in a sustainable manner is a formidable challenge. Although the biological nanomachinery for photosynthetic energy conversion has been remarkably conserved during billions of years of evolution, it is based on a limited set of molecular components that are enabled for their required functions of light harvesting and charge separation by their embedding in a responsive matrix. When the principles of biologically engineered natural photosynthesis are fully elucidated, the design of artificial nanomachinery for sustainable solar fuels may become a reality. Chlorophylls are the principal cofactors involved in both light harvesting and charge separation, and it is their embedding in the protein matrix and shaping by the protein environment that determine the specificity of photosynthetic protein complexes for light harvesting or charge separation. That the same class of moderately sized cofactors can support both functions is not only intriguing, but also paradigmatic of how functional diversity in artificial, semisynthetic dye assemblies can be achieved for solar fuel inspired by the natural systems (26).

SUMMARY POINTS

1. Although the biological nanomachinery for photosynthetic energy conversion has been remarkably conserved during billions of years of evolution, it is based on a limited set of molecular components that are chemically programmed for their required functions of light harvesting and charge separation. Optimization of exciton transfer properties in antennae and charge transfer properties in RCs proceeds by shaping cofactors and by embedding them into responsive protein matrices to tune the electronic and vibrational structure.

2. An important common denominator in photosynthesis is the similar architecture of RCs; in contrast, antenna systems are much more diverse and provide information about different approaches to chemical preprogramming of cofactors for their function.

3. Computational integration of NMR and cryo-EM has revealed that chlorosomes are built from coaxial cylinders of BChl with functional heterogeneity from dislocations. Although chlorosomes are protein free, their biophysics is quite rich, with essential elements of exciton delocalization, of charge separation by proton-coupled electron transfer, and possibly of redox tuning encoded in strained, self-assembled supramolecular entities that are ready for biological engineering in evolution.

4. Protein-induced constraints on the B850 BChl-His motifs in the LH2 antennae leads to considerable mutual charge transfer, with ~ -0.5 e on the BChl, that affects the site energy and dipole transition moments.

5. The axial histidines of the special pair (P) in the BRC of *Rhodobacter sphaeroides* balance the asymmetry in the ground state and produce a $P_L^{\delta-}P_M^{\varepsilon-}$ charge-transfer character that oscillates between the two halves of P and promotes asymmetric electron transfer upon excitation.

6. Rotation of the axial histidines upon excitation of a photosynthetic RC can selectively lower the energy of chlorophyll in plants and bacteria. Molecular dynamics analyses of *R. sphaeroides* reveal classically coherent motion along a collective mode at $\sim 100 \, cm^{-1}$, where rotation of a coordinating His side chain leads to symmetry breaking by a unidirectional displacement of electron density to establish a strong $P_L^+P_M^-$ charge-transfer character in the excited state.

7. Facilitating electron tunneling into a charge-separated state by coupling electronic excitation with a selective vibration induced by a responsive matrix may become a general design principle in artificial photosynthesis.

DISCLOSURE STATEMENT

The authors are not aware of any affiliations, memberships, funding, or financial holdings that might be perceived as affecting the objectivity of this review.

ACKNOWLEDGMENTS

LITERATURE CITED

1. Alia A, Matysik J, De Boer I, Gast P, van Gorkom H, de Groot H. 2004. Heteronuclear 2D (H-1-C-13) MAS NMR resolves the electronic structure of coordinated histidines in light-harvesting complex II: assessment of charge transfer and electronic delocalization effect. *J. Biomol. NMR* 28:157–64

2. **Alia A, Matysik J, Soede-Huijbregts C, Baldus M, Raap J, et al. 2001. Ultrahigh field MAS NMR dipolar correlation spectroscopy of the histidine residues in light-harvesting complex II from photosynthetic bacteria reveals partial internal charge transfer in the B850/His complex. *J. Am. Chem. Soc.* 123:4803–9**

3. **Alia A, Wawrzyniak PK, Janssen GJ, Buda F, Matysik J, de Groot HJM. 2009. Differential charge polarization of axial histidines in bacterial reaction centers balances the asymmetry of the special pair. *J. Am. Chem. Soc.* 131:9626–27**

4. Allen JP, Cordova JM, Jolley CC, Murray TA, Schneider JW, et al. 2009. EPR, ENDOR, and special TRIPLE measurements of $P^{\ast+}$ in wild type and modified reaction centers from *Rb. sphaeroides*. *Photosynth. Res.* 99:1–10

5. Bahatyrova S, Frese RN, Siebert CA, Olsen JD, van der Werf KO, et al. 2004. The native architecture of a photosynthetic membrane. *Nature* 430:1058–62

2. First assessment of the BChl$^{\delta-}$-His$^{\delta+}$ partial charge transfer motif emerging from MAS NMR as a common denominator across antennae and RCs.

3. Symmetry breaking between BChl$^{\delta-}$-His$^{\delta+}$ motifs forming P is associated with hydrogen bonding in the protein responsive matrix.

6. Balaban TS, Holzwarth AR, Schaffner K, Boender GJ, de Groot HJM. 1995. CP-MAS ^{13}C-NMR dipolar correlation spectroscopy of ^{13}C-enriched chlorosomes and isolated bacteriochlorophyll *c* aggregates of *Chlorobium tepidum*: The self-organization of pigments is the main structural feature of chlorosomes. *Biochemistry* 34:15259–66

7. Blankenship RE. 2002. *Molecular Mechanisms of Photosynthesis*. Oxford, UK: Blackwell Sci.

8. Bryant DA, Frigaard N-U. 2006. Prokaryotic photosynthesis and phototrophy illuminated. *Trends Microbiol.* 14:488–96

9. Buda F. 2009. Introduction to theory/modeling methods in photosynthesis. *Photosynth. Res.* 102:437–41

10. Cherepy NJ, Shreve AP, Moore LJ, Boxer SG, Mathies RA. 1997. Temperature dependence of the Qy resonance Raman spectra of bacteriochlorophylls, the primary electron donor, and bacteriopheophytins in the bacterial photosynthetic reaction center. *Biochemistry* 36:8559–66

11. Closs GL, Closs LE. 1969. Induced dynamic nuclear spin polarization in photoreductions of benzophenone by toluene and ethylbenzene. *J. Am. Chem. Soc.* 91:4549–50

12. Cogdell RJ, Isaacs NW, Howard TD, McLuskey K, Fraser NJ, Prince SM. 1999. How Photosynthetic Bacteria Harvest Solar Energy. *J. Bacteriol.* 181:3869–79

13. Creemers A, Kiihne S, Bovee-Geurts P, DeGrip W, Lugtenburg J, de Groot H. 2002. H-1 and C-13 MAS NMR evidence for pronounced ligand-protein interactions involving the ionone ring of the retinylidene chromophore in rhodopsin. *Proc. Natl. Acad. Sci. USA* 99:9101–6

14. Daviso E, Prakash S, Alia A, Gast P, Neugebauer J, et al. 2009. The electronic structure of the primary electron donor of reaction centers of purple bacteria at atomic resolution as observed by photo-CIDNP ^{13}C NMR. *Proc. Natl. Acad. Sci. USA* 106:22281–86

15. de Groot HJM. 2011. Engineering natural photosynthesis. In *Fundamentals of Materials for Energy and Environmental Sustainability*, ed. D Ginley, D Cahen, pp. 365–78. New York: Cambridge Univ. Press

16. Deisenhofer J, Epp O, Miki K, Huber R, Michel H. 1985. Structure of the protein subunits in the photosynthetic reaction centre of *Rhodopseudomonas viridis* at 3Å resolution. *Nature* 318:618–24

17. Diller A, Roy E, Gast P, van Gorkom HJ, de Groot HJM, et al. 2007. ^{15}N photochemically induced dynamic nuclear polarization magic-angle spinning NMR analysis of the electron donor of photosystem II. *Proc. Natl. Acad. Sci. USA* 104:12767–71

18. Eisenmayer TJ, de Groot HJM, van de Wetering E, Neugebauer J, Buda F. 2012. Mechanism and reaction coordinate of directional charge separation in bacterial reaction centers. *J. Phys. Chem. Lett.* 3:694–97

19. Ermler U, Fritzsch G, Buchanan SK, Michel H. 1994. Structure of the photosynthetic reaction centre from *Rhodobacter sphaeroides* at 2.65 Å resolution: cofactors and protein-cofactor interactions. *Structure* 2:925–36

20. Ferreira KN, Iverson TM, Maghlaoui K, Barber J, Iwata S. 2004. Architecture of the photosynthetic oxygen-evolving center. *Science* 303:1831–38

21. Förster T. 1965. Delocalized excitation and excitation transfer. In *Modern Quantum Chemistry*, ed. O Sinanoglu, pp. 93–137. New York: Academic

22. Frigaard NU, Bryant DA. 2006. Chlorosomes: antenna organelles in photosynthetic green bacteria. In *Microbiology Monographs*, ed. JM Shively, pp. 79–114. Berlin: Springer

23. Fromme P, ed. 2008. *Photosynthetic Protein Complexes*. Weinheim, Ger.: Wiley-VCH. 386 pp.

24. Ganapathy S, Oostergetel G, Reus M. 2012. Structural variability in wild-type and bchQ bchR mutant chlorosomes of the green sulfur bacterium *Chlorobaculum tepidum*. *Biochemistry* 51:4488–98

25. Ganapathy S, Oostergetel GT, Wawrzyniak PK, Reus M, Gomez Maqueo Chew A, et al. 2009. Alternating *syn-anti* bacteriochlorophylls form concentric helical nanotubes in chlorosomes. *Proc. Natl. Acad. Sci. USA* 106:8525–30

26. Ganapathy S, Sengupta S, Wawrzyniak PK, Huber V, Buda F, et al. 2009. Zinc chlorins for artificial light-harvesting self-assemble into antiparallel stacks forming a microcrystalline solid-state material. *Proc. Natl. Acad. Sci. USA* 106:11472–77

14. Shows the relation between spatial and electronic structures for ground and excited states of P resolved with photo-CIDNP MAS NMR.

15. Explores the relation between thermodynamics of solar energy conversion and the basic architectures of photosynthetic antenna and RC complexes.

18. Describes the dynamics of the special pair in the BRC in the ground state and how symmetry breaking for charge separation in the excited state is established by classically coherent dynamics.

23. Provides a comprehensive overview of the structural basis of photosynthesis that has been established over three decades with X-ray diffraction.

25. Computational integration of imaging with NMR for structure determination of chlorosomes and a perspective on how chlorophylls interact for photosynthesis.

27. **Giacometti G, Giacometti GM. 2010. Evolution of photosynthesis and respiration: Which came first?** *Appl. Magn. Reson.* 37:13–25

28. Gomez Maqueo Chew A, Frigaard NU, Bryant DA. 2007. Bacteriochlorophyllide *c* C-8^2 and C-12^1 methyltransferases are essential for adaptation to low light in *Chlorobaculum tepidum*. *J. Bacteriol.* 189:6176–84

29. Heller BA, Holten D, Kirmaier C. 1995. Control of electron transfer between the L- and M-sides of photosynthetic reaction centers. *Science* 269:940–45

30. Hill A. 1956. Why biophysics? *Science* 124:1233–37

31. Hoff A, Deisenhofer J. 1997. Photophysics of photosynthesis. Structure and spectroscopy of reaction centers of purple bacteria. *Phys. Rep.* 287:1–247

32. Horton P, Ruban AV, Wentworth M. 2000. Allosteric regulation of the light-harvesting system of photosystem II. *Philos. Trans. R. Soc. Lond. Ser. B* 355:1361–70

33. Hu XC, Damjanovic A, Ritz T, Schulten K. 1998. Architecture and mechanism of the light-harvesting apparatus of purple bacteria. *Proc. Natl. Acad. Sci. USA* 95:5935–41

34. Janssen GJ, Daviso E, van Son M, de Groot HJM, Alia A, Matysik J. 2010. Observation of the solid-state photo-CIDNP effect in entire cells of cyanobacteria *Synechocystis*. *Photosynth. Res.* 104:275–82

35. Jeschke G. 1997. Electron–electron–nuclear three-spin mixing in spin-correlated radical pairs. *J. Chem. Phys.* 106:10072

36. Jeschke G. 1998. A new mechanism for chemically induced dynamic nuclear polarization in the solid state. *J. Am. Chem. Soc.* 120:4425–29

37. Kammel M, Kern J, Lubitz W, Bittl R. 2003. Photosystem II single crystals studied by transient EPR: the light-induced triplet state. *Biochim. Biophys. Acta* 1605:47–54

38. Kanchanawong P, Dahlbom MG, Treynor TP, Reimers JR, Hush NS, Boxer SG. 2006. Charge delocalization in the special-pair radical cation of mutant reaction centers of *Rhodobacter sphaeroides* from Stark spectra and nonadiabatic spectral simulations. *J. Phys. Chem. B* 110:18688–702

39. Kaptein R, Oosterhoff JL. 1969. Chemically induced dynamic nuclear polarization II. *Chem. Phys. Lett.* 4:195–97

40. Kim H, Li H, Maresca JA, Bryant DA, Savikhin S. 2007. Triplet exciton formation as a novel photoprotection mechanism in chlorosomes of *Chlorobium tepidum*. *Biophys. J.* 93:192–201

41. Lubitz W, Lendzian F, Bittl R. 2002. Radicals, radical pairs and triplet states in photosynthesis. *Acc. Chem. Res.* 35:313–20

42. Maresca JA, Gomez Maqueo Chew A, Ponsatí MR, Frigaard N-U, Ormerod JG, Bryant DA. 2004. The *bchU* gene of *Chlorobium tepidum* encodes the C-20 methyltransferase in bacteriochlorophyll *c* biosynthesis. *J. Bacteriol.* 186:2558–66

43. Matthews BW, Fenna RE, Bolognesi MC, Schmid MF, Olson JM. 1979. Structure of a bacteriochlorophyll *a*-protein from the green photosynthetic bacterium *Prosthecochloris aestuarii*. *J. Mol. Biol.* 131:259–85

44. Matysik J, Alia A, Gast P, van Gorkom HJ, Hoff AJ, de Groot HJM. 2000. Photochemically induced nuclear spin polarization in reaction centers of photosystem II observed by ^{13}C-solid-state NMR reveals a strongly asymmetric electronic structure of the P$_{680}^{\cdot+}$ primary donor chlorophyll. *Proc. Natl. Acad. Sci. USA* 97:9865–70

45. Matysik J, Diller A, Roy E, Alia A. 2009. The solid-state photo-CIDNP effect. *Photosynth. Res.* 102:427–35

46. McDermott G, Prince SM, Freer AA, Hawthornthwaite-Lawless AM, Papiz MZ, et al. 1995. Crystal structure of an integral membrane light-harvesting complex from photosynthetic bacteria. *Nature* 374:517–21

47. Moore LJ, Zhou H, Boxer SG. 1999. Excited-state electronic asymmetry of the special pair in photosynthetic reaction center mutants: absorption and Stark spectroscopy. *Biochemistry* 38:11949–60

48. Neal S, Nip AM, Zhang H, Wishart DS. 2003. Rapid and accurate calculation of protein ^{1}H, ^{13}C and ^{15}N chemical shifts. *J. Biomol. NMR* 26:215–40

49. **Novoderezhkin V, Yakovlev A, van Grondelle R, Shuvalov V. 2004. Coherent nuclear and electronic dynamics in primary charge separation in photosynthetic reaction centers: a redfield theory approach.** *J. Phys. Chem. B* 108:7445–57

50. Novoderezhkin VI, van Grondelle R. 2010. Physical origins and models of energy transfer in photosynthetic light-harvesting. *Phys. Chem. Chem. Phys.* 12:7352–65

27. Discusses a paradigm shift for the description of evolution of photosynthesis against the background of a common architecture for the two classes of RC protein complexes.

49. Presents an evidence-based model Hamiltonian description of the dynamics of the charge separation events in the BRC.

51. **Noy D, Moser CC, Dutton PL. 2006. Design and engineering of photosynthetic light-harvesting and electron transfer using length, time, and energy scales. *Biochim. Biophys. Acta* 1757:90–105**

> 51. Explains the relation between photosynthetic architecture and the photochemistry of light harvesting, charge separation, and catalysis at increasingly longer timescales.

52. Pandit A, de Groot HJM. 2012. Solid-state NMR applied to photosynthetic light-harvesting complexes. *Photosynth. Res.* 111:219–26

53. Pandit A, de Groot HJM, Holzwarth A. 2008. *Harnessing solar energy for the production of clean fuels*. Work. Pap. Eur. Sci. Found.

54. Pandit A, Wawrzyniak PK, van Gammeren AJ, Buda F, Ganapathy S, de Groot HJM. 2010. Nuclear magnetic resonance secondary shifts of a light-harvesting 2 complex reveal local backbone perturbations induced by its higher-order interactions. *Biochemistry* 49:478–86

55. Polenova T, McDermott AE. 1999. A coherent mixing mechanism explains the photoinduced nuclear polarization in photosynthetic reaction centers. *J. Phys. Chem. B* 103:535–38

56. Potter J, Fyfe P, Frolov D, Wakeham M, van Grondelle R, et al. 2005. Strong effects of an individual water molecule on the rate of light-driven charge separation in the *Rhodobacter sphaeroides* reaction center. *J. Biol. Chem.* 280:27155–64

57. Prakash S, Alia A, Gast P, de Groot HJM, Jeschke G, Matysik J. 2005. Magnetic field dependence of photo-CIDNP MAS NMR on photosynthetic reaction centers of *Rhodobacter sphaeroides* WT. *J. Am. Chem. Soc.* 127:14290–98

58. Prakash S, Alia A, Gast P, de Groot HJM, Matysik J, Jeschke G. 2006. Photo-CIDNP MAS NMR in intact cells of *Rhodobacter sphaeroides* R26: molecular and atomic resolution at nanomolar concentration. *J. Am. Chem. Soc.* 128:12794–99

59. Prince SM, Papiz MZ, Freer AA, McDermott G, Hawthornthwaite-Lawless AM, et al. 1997. Apoprotein structure in the LH2 complex from *Rhodopseudomonas acidophila* strain 10050: modular assembly and protein pigment interactions. *J. Mol. Biol.* 268:412–23

60. Prokhorenko VI, Steensgaard DB, Holzwarth AR. 2003. Exciton theory for supramolecular chlorosomal aggregates: 1. Aggregate size dependence of the linear spectra. *Biophys. J.* 85:3173–86

61. Reddy N, Kolaczkowski S, Small G. 1993. A photoinduced persistent structural transformation of the special pair of a bacterial reaction center. *Science* 260:68–71

62. Rigby SEJ, Nugent JHA, O'Malley PJ. 1994. ENDOR and special triple resonance studies of chlorophyll cation radicals in photosystem 2. *Biochemistry* 33:10043–50

63. Rischel C, Spiedel D, Ridge JP, Jones MR, Breton J, et al. 1998. Low frequency vibrational modes in proteins: changes induced by point-mutations in the protein-cofactor matrix of bacterial reaction centers. *Proc. Natl. Acad. Sci. USA* 95:12306–11

64. Roszak AW, Gardiner AT, Isaacs NW, Cogdell RJ. 2007. Brominated lipids identify lipid binding sites on the surface of the reaction center from *Rhodobacter sphaeroides*. *Biochemistry* 46:2909–16

65. Roy E, Alia A, Gast P, van Gorkom H, de Groot HJM, et al. 2007. Photochemically induced dynamic nuclear polarization in the reaction center of the green sulphur bacterium *Chlorobium tepidum* observed by ^{13}C MAS NMR. *Biochim. Biophys. Acta* 1767:610–15

66. Roy E, Rohmer T, Gast P, Jeschke G, Alia A, Matysik J. 2008. Characterization of the primary radical pair in reaction centers of *Heliobacillus mobilis* by ^{13}C photo-CIDNP MAS NMR. *Biochemistry* 47:4629–35

67. Sai Sankar Gupta KB. 2011. *Spin torch experiments observed in reaction centers of* Rhodobacter sphaeroides. PhD thesis. Leiden Univ. 142 pp.

68. Spiedel D, Roszak AW, McKendrick K, McAuley KE, Fyfe PK, et al. 2002. Tuning of the optical and electrochemical properties of the primary donor bacteriochlorophylls in the reaction centre from *Rhodobacter sphaeroides*: spectroscopy and structure. *Biochim. Biophys. Acta* 1554:75–93

69. Thamarath SS, Bode BE, Prakash S, Sai Sankar Gupta KB, Alia A, et al. 2012. Electron spin density distribution in the special pair triplet of *Rhodobacter sphaeroides* R26 revealed by magnetic field dependence of the solid-state photo-CIDNP effect. *J. Am. Chem. Soc.* 134:5921–30

70. van Gammeren AJ, Buda F, Hulsbergen FB, Kiihne S, Hollander JG, et al. 2005. Selective chemical shift assignment of B800 and B850 bacteriochlorophylls in uniformly [^{13}C,^{15}N]-labeled light-harvesting complexes by solid-state NMR spectroscopy at ultra-high magnetic field. *J. Am. Chem. Soc.* 127:3213–19

71. van Gorkom HJ. 1986. Photochemistry of photosynthetic reaction centres. *Bioelectrochem. Bioenerg.* 16:77–87

72. Wawrzyniak PK, Alia A, Schaap RG, Heemskerk MM, de Groot HJM, Buda F. 2008. Protein-induced geometric constraints and charge transfer in bacteriochlorophyll-histidine complexes in LH2. *Phys. Chem. Chem. Phys.* 10:6971–78

73. Wawrzyniak PK, Beerepoot MTP, de Groot HJM, Buda F. 2011. Acetyl group orientation modulates the electronic ground-state asymmetry of the special pair in purple bacterial reaction centers. *Phys. Chem. Chem. Phys.* 13:10270–79

74. Wirtz AC, van Hemert MC, Lugtenburg J, Frank HA, Groenen EJJ. 2007. Two stereoisomers of spheroidene in the *Rhodobacter sphaeroides* R26 reaction center: a DFT analysis of resonance Raman spectra. *Biophys. J.* 93:981–91

75. Wishart DS, Sykes BD, Richards FM. 1991. Relationship between nuclear magnetic resonance chemical shift and protein secondary structure. *J. Mol. Biol.* 222:311–33

76. Zech SG, Kurreck J, Eckert HJ, Renger G, Lubitz W, Bittl R. 1997. Pulsed EPR measurement of the distance between $P_{680}^{+\cdot}$ and $Q_A^{-\cdot}$ in photosystem II. *FEBS Lett.* 414:454–56

77. Zouni A, Witt HT, Kern J, Fromme P, Krauss N, et al. 2001. Crystal structure of photosystem II from *Synechococcus elongatus* at 3.8 Å resolution. *Nature* 409:739–43

78. Zysmilich M, McDermott A. 1994. Photochemically induced dynamic nuclear polarization in the solid-state ^{15}N spectra of reaction centers from photosynthetic bacteria *Rhodobacter sphaeroides* R-26. *J. Am. Chem. Soc.* 116:8362–63